

# H-NS Oligomerization Domain Structure Reveals the Mechanism for High Order Self-association of the Intact Protein

Diego Esposito<sup>1</sup>, Arsen Petrovic<sup>1</sup>, Richard Harris<sup>1</sup>, Shusuke Ono<sup>1</sup>  
John F. Eccleston<sup>2</sup>, Amina Mbabaali<sup>2</sup>, Ihtshamul Haq<sup>1</sup>  
Christopher F. Higgins<sup>3</sup>, Jay C. D. Hinton<sup>4</sup>, Paul C. Driscoll<sup>1,5</sup> and  
John E. Ladbury<sup>1\*</sup>

<sup>1</sup>Department of Biochemistry  
and Molecular Biology  
University College London  
Darwin Building, Gower Street  
London WC1E 6BT, UK

<sup>2</sup>National Institute for Medical  
Research, The Ridgeway, Mill  
Hill, London NW7 1AA, UK

<sup>3</sup>Faculty of Medicine, MRC  
Clinical Sciences Centre  
Imperial College, Hammersmith  
Hospital Campus, DuCane  
Road, London W12 0NN, UK

<sup>4</sup>Institute for Food Research  
Norwich Research Park, Colney  
Norwich NR4 7UA, UK

<sup>5</sup>Ludwig Institute for Cancer  
Research, 91 Riding House  
Street, London W1W 7BS, UK

H-NS plays a role in condensing DNA in the bacterial nucleoid. This 136 amino acid protein comprises two functional domains separated by a flexible linker. High order structures formed by the N-terminal oligomerization domain (residues 1–89) constitute the basis of a protein scaffold that binds DNA *via* the C-terminal domain. Deletion of residues 57–89 or 64–89 of the oligomerization domain precludes high order structure formation, yielding a discrete dimer. This dimerization event represents the initial event in the formation of high order structure. The dimers thus constitute the basic building block of the protein scaffold. The three-dimensional solution structure of one of these units (residues 1–57) has been determined. Activity of these structural units is demonstrated by a dominant negative effect on high order structure formation on addition to the full length protein. Truncated and site-directed mutant forms of the N-terminal domain of H-NS reveal how the dimeric unit self-associates in a head-to-tail manner and demonstrate the importance of secondary structure in this interaction to form high order structures. A model is presented for the structural basis for DNA packaging in bacterial cells.

© 2002 Elsevier Science Ltd. All rights reserved

\*Corresponding author

**Keywords:** chromatin; coiled-coil; DNA packaging; nucleoid assembly; histone-like

## Introduction

Several proteins interact with DNA in the bacterial nucleoid to facilitate chromosome condensation and modulate gene expression. H-NS is one of the most abundant components of bacterial chromatin.<sup>1–6</sup> H-NS is a 15.6 kDa, 136 amino acid protein that is present at high copy number (up to

10<sup>5</sup> molecules) in cells of all Enterobacteriaceae. Several studies have investigated the role of H-NS in the modulation of DNA super-coiling and the control of gene expression,<sup>5,7</sup> but a structural model of the intact H-NS molecule has yet to evolve.

Full length H-NS forms concentration-dependent, self-associated, high order, complexes.<sup>8,9</sup> The protein is composed of two distinct domains: the N-terminal domain mediates protein oligomerization, and the C-terminal domain is required for non-sequence specific DNA binding.<sup>7,8,10–12</sup> These domains are separated by a flexible linker that provides the C-terminal domain with a freedom of movement relative to the oligomeric N-terminal domain.<sup>9</sup> Residues 1–89 are necessary and sufficient for higher-order oligomerization.<sup>9</sup> In contrast, a truncated version of this domain (residues 1–64; H-NS<sub>1–64</sub>) was shown to

Abbreviations used: H-NS, wild-type from *Salmonella typhimurium* with the C at position 20 replaced by a S; H-NS<sub>1–57</sub>, H-NS<sub>1–64</sub>, the first 57 or 64 residues of H-NS but also including the GSHM-tag derived from the cloning vector; NOE, nuclear Overhauser effect; HSQC, heteronuclear single quantum correlation.

E-mail address of the corresponding author:  
[j.ladbury@biochem.ucl.ac.uk](mailto:j.ladbury@biochem.ucl.ac.uk)

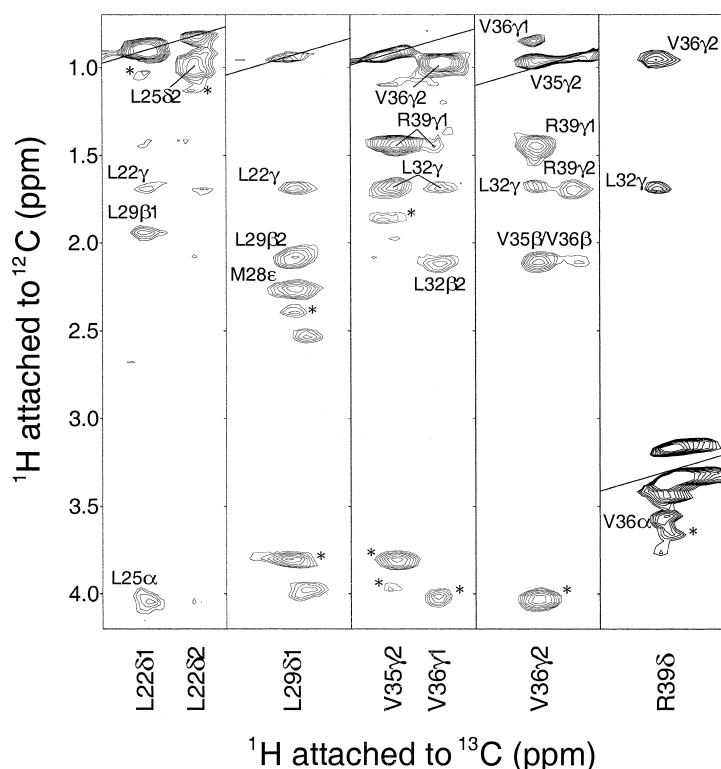


**Figure 1.** Inter-chain connectivities. Examples of strips taken from the 3D  $^{13}\text{C}$   $F_1$ -filtered,  $F_3$ -edited NOESY-HSQC spectrum ( $\tau_m = 100$  ms) recorded on a 1:1 mixture  $^{13}\text{C}/^{15}\text{N}$  and  $^{12}\text{C}/^{14}\text{N}$  (natural isotope abundance) labelled H-NS $_{1-57}$ , illustrating inter-chain NOEs for the coiled coil region. Cross-peaks that are labelled \* could not be assigned unambiguously.

have a defined oligomeric state that is largely  $\alpha$ -helical and was likely to self-associate *via* a coiled-coil interaction. Thus, residues 1–64 can be considered to form a basic building block, while residues from 65 to 89 appear to be responsible, at least in part, for the formation of the higher-order structures.<sup>9</sup>

A H-NS $_{1-64}$  protomer, within the context of its defined oligomeric state, was previously shown by NMR to consist of three helices separated by short linkers.<sup>13</sup> Residues 54–64 form a largely unstructured, dynamic region. Here we report the three dimensional structure of residues 1–57 which in their dimeric state represent part of the basic building block for the high order self-assembly of H-NS. The largest helix (H3) forms a parallel coiled-coil interface whilst the N-terminal helices H1 and H2 lie approximately anti-parallel with H3 and make both intra- and inter-molecular interactions to the coiled-coil core. Investigation of the formation of the high-order, heterodispersed complexes by self-assembly of the N-terminal domain suggest a model whereby the high order protein scaffold is formed *via* a head-to-tail (i.e. N terminus to C terminus) interaction of the component dimeric units. This result provides the basis for understanding how H-NS can facilitate the packaging of chromosomal DNA in the bacterial cell.

## Results

### The solution structure of residues 1–57 of the H-NS oligomerization domain

We have previously shown by heteronuclear NMR spectroscopy that the residues towards the

C terminus of H-NS $_{1-64}$  exhibited characteristics of high internal mobility, suggesting a dynamically disordered conformation with no well-defined secondary structure.<sup>13</sup> Furthermore, these residues yielded NMR resonances with strong overlap in the NMR spectrum. As a result we expressed an H-NS polypeptide comprising just the N-terminal residues 1–57, H-NS $_{1-57}$ , for further NMR studies and solution structure determination. Sedimentation equilibrium analytical ultracentrifugation (AUC) experiments established that H-NS $_{1-57}$  is a homodimer (as with the 1–64 construct, see below). The 2D [ $^{15}\text{N}$ , $^1\text{H}$ ]-heteronuclear single quantum coherence (HSQC) spectrum of isotope labelled H-NS $_{1-57}$  retains the main features previously observed for H-NS $_{1-64}$ ,<sup>13</sup> but with fewer cross-peaks, enhanced spectral resolution, and reduced cross-peak overlap.  $^{15}\text{N}$  nuclear relaxation data were recorded to obtain residue-by-residue  $R_1$ ,  $R_2$  relaxation rates and  $\{^1\text{H}\}^{15}\text{N}$  heteronuclear NOEs. The model-free formalism-derived estimate of the molecular rotational correlation time  $\tau_c \sim 11$  ns is consistent with a molecular entity that reorients more rapidly than H-NS $_{1-64}$ .<sup>14</sup> A double  $^{15}\text{N}/^{13}\text{C}$ -isotope labelled H-NS $_{1-57}$  sample was used in a standard set of triple resonance experiments to obtain sequence-specific resonance assignments using a strategy similar that reported previously for H-NS $_{1-64}$ ,<sup>13</sup> except that perdeuteration of the protein was not required. The high  $\alpha$ -helical content of H-NS $_{1-57}$ , combined with the absence of aromatic side-chains, gives rise to relatively poor dispersion of the  $\text{C}^\alpha$  and  $\text{H}^\alpha$  chemical shifts making the side-chain resonance assignments difficult to obtain. Nevertheless these assignments were determined by analysis of

**Table 1.** Summary of structure statistics

	(SA)	Closest to mean structure
<i>Experimental restraint<sup>a</sup></i>		
All (Å) (1560)	0.075 ± 0.006	0.073
Unambiguous (Å) (969)	0.074 ± 0.009	0.069
Ambiguous (Å) (483)	0.076 ± 0.003	0.081
Hydrogen bond restraints (Å) (108)	0.090 ± 0.007	0.076
Dihedral angle restraints (deg.) (156)	0.43 ± 0.07	0.56
<i>Number of residual restraints violations<sup>b</sup></i>		
NOE violations > 0.5 Å	0.45 ± 0.5	0
NOE violations > 0.4 Å	3.7 ± 2.2	6
Angle violations > 3°	2.4 ± 1.5	2
<i>Deviations from idealised covalent geometry<sup>c</sup></i>		
Bonds (Å) (1870)	0.0031 ± 0.0001	0.0033
Angles (deg.) (3394)	0.49 ± 0.01	0.49
Improper (deg.) (888)	0.42 ± 0.09	0.33
<i>Structural statistics for the ensemble<sup>d</sup></i>		
PROCHECK parameters		
Most favoured region (%)	85.9 ± 2.5	85.5
Additionally allowed (%)	7.3 ± 1.6	7.3
Generously allowed (%)	3.8 ± 1.4	3.6
Disallowed (%)	3.0 ± 1.0	3.6
Number of bad contacts	8.8 ± 2.4	6
CHARMM Lennard-Jones energy <sup>e</sup>		
$E_{LJ}$ (kcal mol <sup>-1</sup> )	-923 ± 13	-932
RMSD from the average structure <sup>f</sup>		
Backbone (N, C <sup>α</sup> , C) (Å)	0.39 ± 0.06	
Heavy atoms (Å)	0.91 ± 0.07	

Column 2, (SA), represents the set of 20 selected conformers obtained by simulated annealing. Column 3 represents values relative to the structure which is closest to the regularised mean structure obtained by best fitting and coordinate averaging the (SA) set followed by restrained energy minimisation in the same force field.

<sup>a</sup> Sum averaging of NOE distance restraints was used for groups with degenerate proton chemical shifts. The inter-proton unambiguous distance restraint list comprised 466 intra-residue, 274 sequential ( $|i - j| = 1$ ), 126 short range ( $1 < |i - j| < 5$ ), 103 long-range ( $|i - j| > 5$ ) and inter-chain entries. Hydrogen-bonds restraints were applied as pairs of distance restraints: H<sup>N</sup> → O 1.2 Å–2.2 Å; N → O 1.2–3.2 Å.

<sup>b</sup> No experimental distance restraint was violated by more than 0.6 Å and no angle was violated by more than 5°.

<sup>c</sup> The final values for the respective force constants were: bond lengths, 500 kcal mol<sup>-1</sup> Å<sup>-2</sup>, angles and improper torsions, 500 kcal mol<sup>-1</sup> rad<sup>-2</sup>. The improper torsion angle restraints serve to maintain planarity and chirality.

<sup>d</sup> The program PROCHECK<sup>36</sup> was used to assess the stereochemical parameters of the family of conformers. The Figures indicate the percentage of residues with backbone  $\phi$  and  $\psi$  angles in separate regions of the Ramachandran plot, defined in the program. The number of bad contacts per 100 residues is expected to be in the range 0–30 for protein crystal structures of better than 3.0 Å resolution.

<sup>e</sup> The CHARMM<sup>38</sup> Lennard-Jones van der Waals energy term, which was not included in the force field of the simulated annealing of restrained minimisation, was used to assess the atomic packing of the structure. A negative value is consistent with the absence of any significant atomic clash.

<sup>f</sup> The precision of the atomic coordinates is defined as the average pairwise RMSD between each of the 20 conformers and a mean coordinate structure SA generated by iterative best-fit of the backbone atoms (N, C<sup>α</sup>, and C) over residues 2–48 (comprising the core secondary structure elements and omitting the flexible N and C termini, residues one and residues 49–57) followed by coordinate averaging.

<sup>1</sup>H–<sup>13</sup>C–<sup>13</sup>C–<sup>1</sup>H correlations in a 17 ms mixing time 3D HCCH-TOCSY experiment combined with 2D <sup>13</sup>C,<sup>1</sup>H-HSQC and 3D <sup>13</sup>C-NOESY-HSQC spectra. In contrast to H-NS<sub>1–64r</sub>, the majority of <sup>1</sup>H–<sup>1</sup>H correlations between NH protons and the side-chains could be detected in 3D <sup>15</sup>N-TOCSY-HSQC and <sup>15</sup>N-NOESY-HSQC spectra (mixing times 60 ms and 80 ms, respectively), which greatly assisted the confidence in the accuracy of the assignments. A complete listing of the resonance assignments for H-NS<sub>1–57</sub> has been deposited at the BioMagResBank (Number RCSB016203).

The observed pattern of residue-by-residue secondary <sup>13</sup>C chemical shifts and <sup>15</sup>N nuclear relaxation data is essentially identical for residues 1–48 of H-NS<sub>1–57</sub> and H-NS<sub>1–64r</sub>, indicating that there are no significant differences in the component secondary structural elements. The polypeptide comprises two short  $\alpha$ -helices (H1, residues 2–7; and H2, residues 10–16) followed by a longer third helix (H3, residues 22–49). As with H-NS<sub>1–64r</sub>, we noted that incubation of H-NS<sub>1–57</sub> at room temperature over the course of several weeks yielded evidence, clearly observed in the NMR spectra, of a gradual proteolytic degradation of the sample. Proteolysis occurs primarily at the C-terminal end of the protein, indicating lack of a rigid secondary structure in this region. This phenomenon is consistent with <sup>15</sup>N relaxation and heteronuclear NOEs data that reveal a higher degree of flexibility of residues 50–57, which in H-NS<sub>1–64</sub> appear to be arranged as part of the coiled-coil core helices but showed faster transverse relaxation time-constants compared to the preceding residues in the helix segment.<sup>13</sup> For H-NS<sub>1–57</sub> the chemical shift and heteronuclear relaxation data indicate that ordered helical structure is present up to residue 49.

The 3D solution structure of the H-NS<sub>1–57</sub> homodimer was determined on the basis of inter-proton distance and dihedral angle restraints derived from the NMR data recorded using isotope-labelled samples of the protein. Unambiguous assignment of 101 NOE connectivities between protomers was obtained by analysis of a 3D <sup>13</sup>C F<sub>1</sub>-filtered, F<sub>3</sub>-edited NOESY-HSQC experiment<sup>15</sup> recorded using a sample containing a 1:1 ratio of unlabelled (<sup>12</sup>C/<sup>14</sup>N) and double <sup>13</sup>C/<sup>15</sup>N-isotope labelled chains (Figure 1). NOE cross-peaks observed in 3D <sup>13</sup>C-NOESY-HSQC experiments on fully labelled samples but absent in the 3D <sup>13</sup>C F<sub>1</sub>-filtered, F<sub>3</sub>-edited NOESY-HSQC experiment with mixed labelled and unlabelled chains, were attributed exclusively to intra-chain connectivities.

Structure calculations for the H-NS<sub>1–57</sub> homodimer were performed by dynamical simulated annealing using CNS<sup>16</sup> from random starting conformations, including a restraint term to enforce the molecular symmetry consistent with the observation of a single set of NMR resonances. Table 1 summarises the experimental restraints employed in the structure determination. Figure 2(a) shows a superposition of a number of representative low

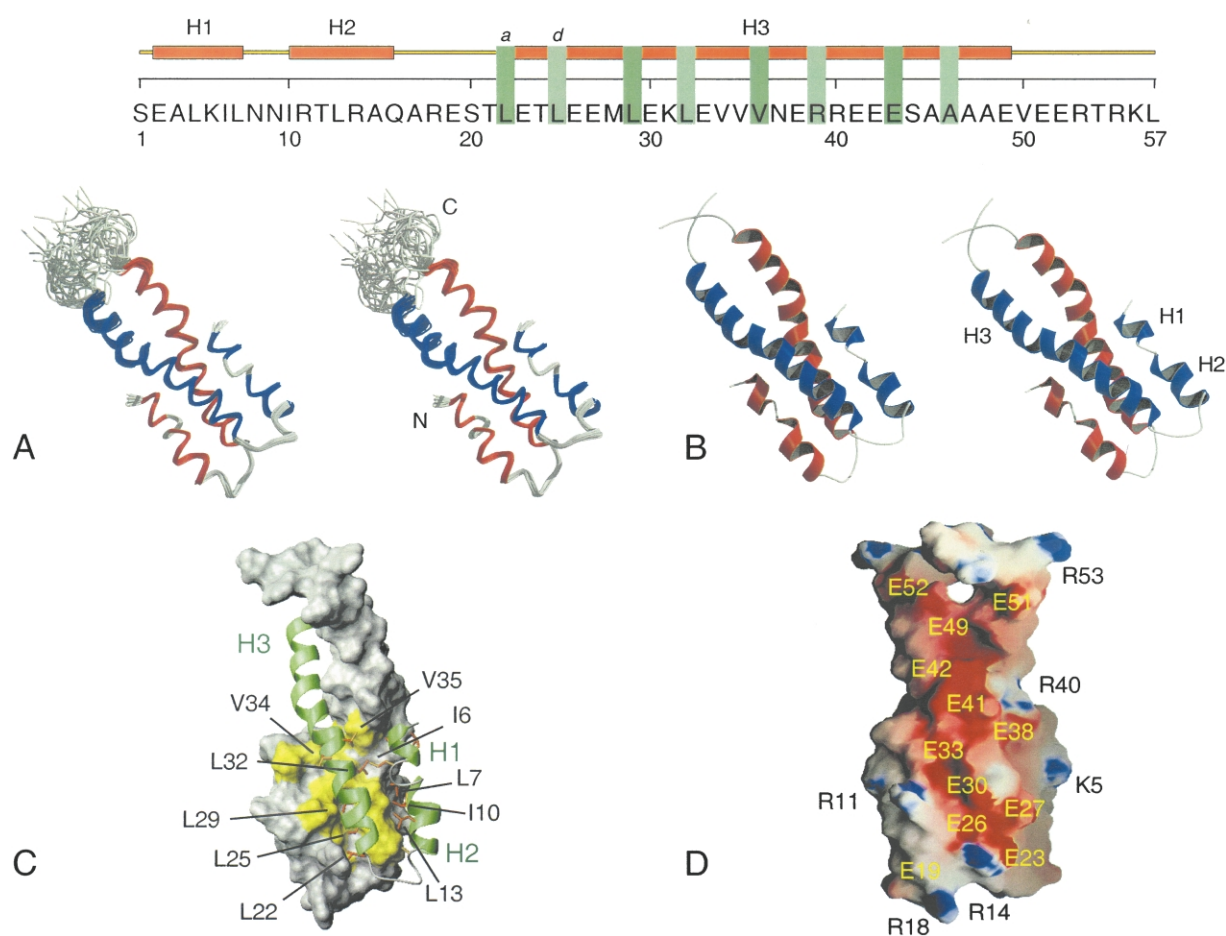
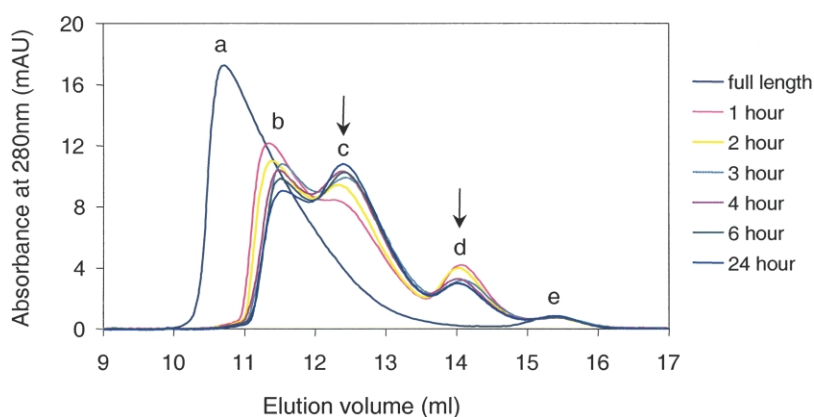


**Figure 2.** (a) Bundle of the 20 lowest energy structures of H-NS<sub>1-57</sub> after least-squares alignment of the backbone and/or heavy atoms. The two protomers are shown in red and blue, respectively. The N and C termini are shown for one of the protomers in the homodimer. (b) Stereo view ribbon diagram of the lowest energy, three dimensional structure of H-NS<sub>1-57</sub>. The two protomers are shown in red and blue, respectively. Helices H1–H3 are shown for one protomer in the homodimer. (c) View of the hydrophobic interactions between the coiled coil (Helix 3) and Helices 1 and 2 on H-NS<sub>1-57</sub>. One protomer is shown with a van der Waals surface representation (grey) whilst the other is displayed as a ribbon structure (green). The hydrophobic residues on the van der Waals surface are shown in yellow, whilst the side-chains of the other protomer extend from the ribbon (orange) and are labelled. (d) The electrostatic surface of H-NS<sub>1-57</sub> shown on van der Waals surface representation of the structure. The structure has a largely negatively charged exterior (red) with few solvent exposed basic residues (blue). Key acidic and basic residues are labelled in yellow and black, respectively. The first 57 residues of H-NS are shown at the top of the page with the secondary structural units highlighted above. The heptad repeat elements are shown in grey.

energy conformers that emerged from the structure calculations. The refinement proceeds with low values of the restraint penalty functions whilst clearly retaining helices H1–H3 with excellent stereochemical properties. The structure is well-defined by the input restraints, and the RMSD values for the converged family of conformers is within the range anticipated for accurate solution structures (see Table 1). The overall shape is globular but non-spherical, with a longest dimension of approximately 50 Å. The overall fold of the H-NS<sub>1-57</sub> homodimer constitutes a left-handed parallel coiled-coil (Helix H3) buttressed by the two smaller helices H1 and H2 at the N terminus that fold back on to the H3 helix from the same protomer (Figure 2(b)). The positions of residues 50–57 are not well defined by the input restraints and appear disordered in the conformer bundle,

consistent with the NMR characteristics for this region described above. Superposition of the backbone coordinates with the solution structure of the c-Myc-Max heterodimer leucine zipper (PDB code 1a93) for the central coiled-coil region (residues 5–31 of the leucine zipper aligned with H-NS<sub>1-57</sub> residues 24–50) yields an RMSD of only about 2.0 Å. The *a* positions of the canonical coiled-coil heptad repeats are occupied by residues Leu22, Leu29, Val36 and Glu43; the *d* positions by residues Leu25, Leu32, Arg39 and Ala46. The guanidinium group of Arg39 is directed to the solvent exposed surface of the protein, and makes an interaction with the more buried carboxyl group of Glu43.

Ile6, Leu7, Ile10 and Leu13 from helices H1 and H2, which “bind back” onto the coiled-coil structure, form a contiguous hydrophobic ridge that fits into the groove between the two H3 helices,



(arrowed) is at an elution volume corresponding to H-NS<sub>1-64</sub>. Peak e is a small amount impurity derived from a degradation product of the full length protein.

the bottom of which is lined by the side-chains of Leu22, Leu25, Leu29 and Leu32 (Figure 2(c)). The Arg14 side-chain of each protomer forms salt bridge interactions with Glu23 and Glu26 of the other chain in an inter-molecular interaction. This contact is consistent with the strong downfield chemical shift observed for the Arg14 <sup>1</sup>H resonance ( $\delta = 9.10$  ppm). The orientation of H1 and H2 on the coiled-coil structure exposes a number of acidic and basic residues at the N terminus of the structure (e.g. Lys5, Arg11, Arg14, Arg18, Glu19). However, the exposed surface of the coiled-coil is dominated by negatively charged residues, which combine to form a contiguous negatively charged patch that runs the length of the molecule (see Figure 2(d)). This region of negative charge would tend to oppose interaction with DNA and thus direct it to the C terminus.

### The truncated N-terminal domain dimer binds full length H-NS

If the truncated N-terminal polypeptide dimer is correctly folded and represents a functional unit it should be able to interact with full length H-NS. Since truncated forms of the protein (i.e. H-NS<sub>1-57</sub> and H-NS<sub>1-64</sub>) are unable to form high order structure, addition of these polypeptides to full length H-NS would be expected to inhibit the formation of high order oligomers, i.e. acting to “cap” the progressive self-assembly. Full length H-NS was incubated for different periods of time and at a range of temperatures with an equimolar concentration of H-NS<sub>1-64</sub>, and the distribution of oligomeric forms measured by analytical size exclusion chromatography (SEC). Typical data for samples incubated at 45 °C (Figure 3) show that the SEC profile changes after addition of H-NS<sub>1-64</sub>. The size of the highest molecular mass species declined (i.e. the elution volume increased) dramatically after one hour of incubation. As the incubation time was increased the maximum size of the high order oligomer (peak a) became progressively lower (peak b). Concomitantly a discrete peak

**Figure 3.** Analytical SEC data showing the effect of the mixing of full length H-NS with the truncated H-NS<sub>1-64</sub> mutant protein, both at 0.04 mM. The lines show the molecular mass profile after incubation of the two polypeptides at 45 °C for different times as indicated in the legend. Peak a corresponds to the maximal size of the full length protein in isolation. Peaks b, and c correspond to the mixtures of full length H-NS and H-NS<sub>1-64</sub>. Peak c (arrowed) is at an elution volume corresponding to a molecular mass of approximately 49 kDa. Peak d

appeared at a lower molecular mass (initially observed as a shoulder on the high molecular mass peak after one hour, but as the major peak after 24 hours incubation (peak c). On the basis of comparison with globular protein standards the species at peak c has a molecular mass of approximately 49 kDa. Since the H-NS<sub>1-64</sub> polypeptide forms a stable dimer (as confirmed by AUC studies, Figure 4) this lower molecular mass species has a molecular mass close to that expected from the formation of a discrete tetramer formed between a homodimer of full length H-NS and a homodimer of H-NS<sub>1-64</sub> (with total predicted molecular mass of approximately 47.8 kDa). Thus, assuming that the dimerization constant for the H3 coiled-coil is high, resulting in stable homodimers, a tetramer represents the minimum complex size formed between full length and truncated H-NS. These data are consistent with dimeric H-NS<sub>1-64</sub> inhibiting the high order self-assembly of the full length protein, and therefore implying its properties have physiological relevance.

### Dimeric oligomerization domains of H-NS assemble to high order structures by head-to-tail interactions

The dimeric H-NS<sub>1-64</sub> constitutes a basic structural unit, which in the presence of the additional C-terminal residues of the oligomerization domain (amino acid residues 65–89) self-assembles to form a high order, heterodisperse oligomer. Because the H-NS<sub>1-64</sub> (and H-NS<sub>1-57</sub>) are limited to forming dimers, high order structure cannot form by interaction of these N-terminal residues alone. To rationalize our observations two mutually exclusive models for self-assembly of these structural units into high order complexes can be proposed. In model 1 the high order structure involves the interaction of the C terminus of one oligomerization domain with the N terminus of another (the “head-to-tail” model). Thus, removal of residues 65–89 would delete, or disrupt the site of interaction and, as observed, preclude

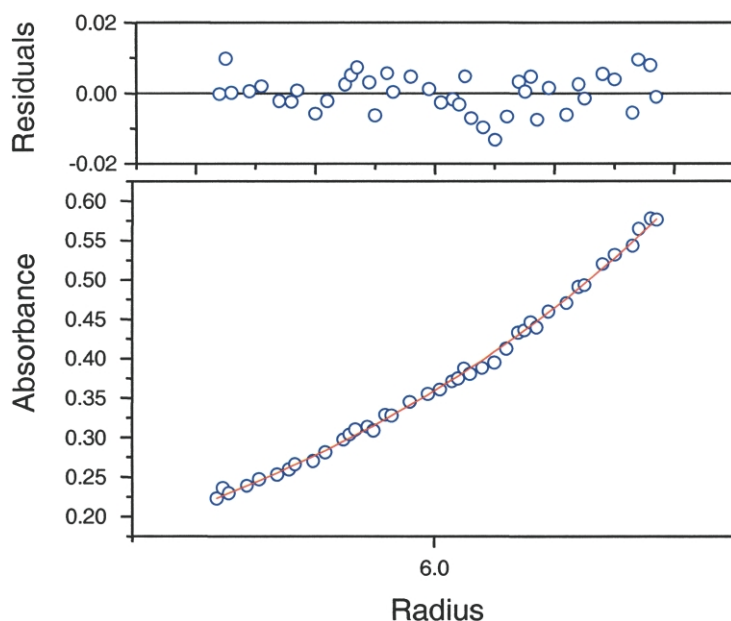


**Figure 4.** AUC sedimentation equilibrium data for H-NS<sub>1-64</sub> in 20 mM Tris-HCl (pH 8.0), 0.3 M NaCl and 5% (w/v) glycerol. Data shown are for a spin speed of 36,000 rpm. All data sets were fitted to a single species model using the calculated partial specific volume of 0.729 and density of 1.0252. The data set shown is that with an initial absorbance of 0.7 at 36,000 rpm. The line corresponds to the best fit to a single species of molecular mass of 14,114 Da. The calculated monomer molecular mass is 7926.9 Da. Above are the residuals between the experimental data and the fitted line.

self-assembly of the H-NS<sub>1-64</sub> dimer to a high order complex. In model 2 the high order oligomer forms through interaction of the residues 65–89 of the oligomerization domain alone. This would, again, be consistent with the observation of discrete homodimer species in the absence of residues 65–89.

The validity of the two models can be tested experimentally by deleting residues from the N terminus of the oligomerization domain as this truncation would be expected to prevent the formation of high order oligomers (i.e. produce a dimer) if model 1 is correct, yet have no effect if dimer–dimer interactions are through the residues 65–89 alone (model 2). Therefore, we examined truncated versions of H-NS in which the first 11 residues were deleted from the oligomerization domain generating H-NS<sub>12-89</sub> that is predicted not to have a disrupted coiled-coil region. Analytical SEC data (Figure 5(a)) showed that H-NS<sub>12-89</sub> exists as a single discrete species with an apparent molecular mass consistent with a homodimeric state similar to that observed for H-NS<sub>1-64</sub>. This interaction was confirmed by AUC data in the concentration range 0.096–0.142 mM (Figure 5(b)). Taken together these data are consistent only with model 1, demonstrating that the high order self-assembly of H-NS oligomerization domains is *via* a head-to-tail association of dimers.

### Helix 2 plays a role in self-assembly of the oligomerization domains

In the head-to-tail interaction, residues at either end of H-NS<sub>1-89</sub> are predicted to be involved in interactions between the dimeric component units. Each H-NS monomer in the dimer has two, short  $\alpha$ -helices H1 and H2 at the N terminus of the protein (Figure 2). To assess the role of these helices in high order complex formation we introduced “helix-disrupting” proline residues into the helices

of H-NS<sub>1-89</sub>. Analytical SEC was used to assess whether the mutations affect the formation of high order, heterodisperse oligomers. A Lys5Pro mutant that disrupts H1 has no discernable effect on oligomerization (i.e. a high order macromolecular assembly was still observed; Figure 5(a)). In contrast, Gln16Pro in H2 gave a single species on SEC equivalent to the dimeric wild-type H-NS<sub>12-89</sub> (see Figure 5(a)). As well as compromising the structural integrity of H2 the Gln16Pro mutant could also affect the formation of the salt bridge between Arg14 and Glu23 and Glu26 residues thereby disturbing the orientation of H2. The importance of the structural integrity of H2 for higher order self-association is further emphasized by the inability of the H-NS<sub>12-89</sub> deletion mutant to form high order complexes. Truncation at residue 12 is likely to seriously compromise the folding of this  $\alpha$ -helix (residues 10–16). It is therefore predicted that H2 is required to form a site for recognition of the C-terminal residues of an adjacent, interacting dimer in the head-to-tail self-association. Hence, disruption of the  $\alpha$ -helix structure and/or position negates head-to-tail oligomerization.

### Discussion

We present a structural model for the high order protein chromosome scaffold formed by the bacterial chromatin structuring protein, H-NS. The principal component of the scaffold is a dimeric oligomerization domain which self-assembles into a heterodisperse high order structure in a head-to-tail manner. The solution structure of the core of this oligomerization domain reveals a dimeric coiled-coil comprised from H3 (residues 22–49), flanked by two N-terminal helices of each protomer. These N-terminal helices (H1, residues 2–7; and H2, 10–16) adopt a conformation whereby they

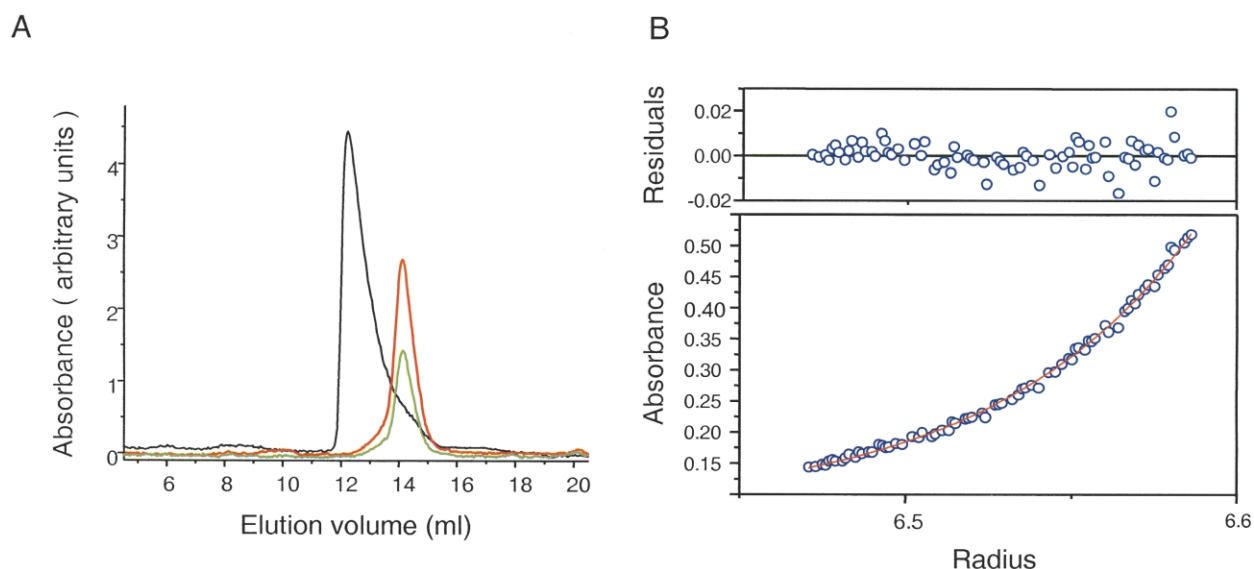


**Figure 5.** (a) Gel filtration assay for H-NS<sub>12-89</sub> at two concentrations; 0.025 mM (in green) and 0.05 mM (in red) at 25 °C. Also shown are data for the full length H-NS with the Lys5Pro mutation (in black). The Figures give the optical density at 220 nm as a function of elution time (minutes). (b) AUC sedimentation equilibrium data for H-NS<sub>12-89</sub>. Two solutions in 2 mM Tris–HCl (pH 8.0), 0.3 M NaCl and 5% glycerol with initial absorbances of 0.4 and 0.7 were allowed to reach equilibrium at 20,000 rpm, 32,000 rpm, 36,000 rpm and 42,000 rpm. All eight data sets were fitted to a single species model using the calculated partial specific volume of 0.729 and density of 1.0252. The data set shown is that with an initial absorbance of 0.7 at 36,000 rpm. The line corresponds to the best fit to a single species of molecular mass of 16,820 Da. The calculated monomer molecular mass is 9258.5 Da. Above are the residuals between the experimental data and the fitted line.

fold back onto the core of the coiled-coil burying a significant hydrophobic surface. The position of these helices is further stabilised by a salt bridge interaction between residue Arg14 and the two acidic residues, Glu23 and Glu26. The integrity of the structure and/or orientation of the second of these helices, H2, are required for high order oligomerization. It is likely that H2 presents a binding site for the C terminus of another adjacent oligomerization domain that interacts in a head-to-tail manner.

The structure for the domain detailed here is consistent with previous experimental observations. Mutational studies *in vivo*<sup>11</sup> indicated that H-NS has three functional domains; the N-terminal (approximately) 20 amino acid residues are responsible for gene repression/silencing; residues 22–64 are required for dimerization, and the C-terminal residues form the DNA binding domain. Clearly the present study provides a structural basis for interpretation of these genetic data for residues 22–64 and the C-terminal domain. Furthermore, the observed gene repression/silencing attributed to residues 1–20 could result from disruption of the capacity to undergo high order self-assembly, correct DNA packaging and hence gene repression if these residues are perturbed. Here we demonstrate that truncated mutants of the oligomerization domain of H-NS cannot oligomerize and are able to interact with the full length protein inhibiting high order structure formation *in vitro*. This is consistent with the dominant negative phenotype observed for similar genetic deletions.<sup>8,12</sup> Mutation of Arg11 (our numbering) to Cys or His did not

affect H-NS oligomerization<sup>8</sup> or secondary structural content.<sup>17</sup> This is as our structural data would predict, since this residue is solvent exposed and therefore unlikely to affect the interaction with the coiled-coil, or the conformational integrity of H2. Residues Leu25, Leu29 and Ala46 (our numbering) form crucial interactions in the *a* and *d* positions of the heptad repeat explaining why, mutation of the Leu residues to Pro residues,<sup>11,12</sup> or deletion of the Ala,<sup>4</sup> compromise coiled-coil formation and result in the observed loss of function of H-NS. Atomic force microscopy on H-NS–DNA complexes showed that at high concentrations of protein, circular DNA molecules (at a stoichiometry of one protein molecule to three base-pairs) are condensed into rod-like structures.<sup>18</sup> Since no significant differences in height along the DNA interface were observed, these data are consistent with an interaction with a protein filament (suggested by our model) rather than discrete protein oligomers (as seen in eukaryotic nucleosomes).

Biochemical data therefore suggest a structural model for the mode in which H-NS homodimers self-associate to form the high order complex that acts as a scaffold for DNA condensation (Figure 6). Having previously shown that the two domains fold independently and are separated by a flexible linker,<sup>9</sup> our model assumes that the N-terminal 89 residues act independently of the C-terminal DNA binding domain (residues 90–136). The N-terminal 89 residues associate to form a dimer, which then self-assembles, *via* interaction of the N- and

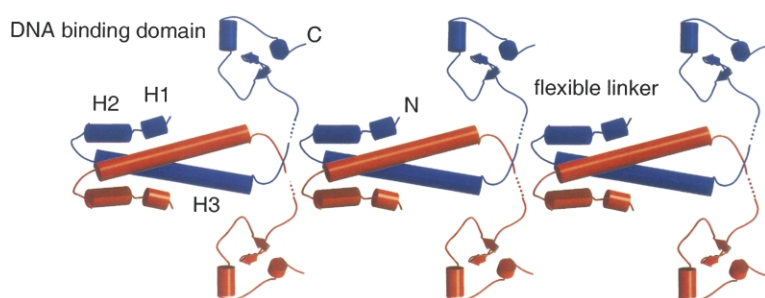


**Figure 6.** Schematic model based on the head-to-tail interaction demonstrated in this work for the self-association of H-NS dimers to form a protein scaffold for association with DNA. Within the context of the full length protein, residues at the C terminus of the dimeric oligomerization domain (including helices H1–H3, see Figure 2) interact with those at the N terminus of a second dimeric oligomerization

domain forming a protein filament. The DNA binding, C-terminal domain extends from the filament on a flexible linker region to enable interaction with DNA (the C-terminal domain was modelled from the homologous *E. coli* structure<sup>35</sup>). The dotted line is undefined structure (i.e. residues 57–89 and residues of the flexible linker region).

C-terminal residues of this core unit, forming a high order, rod-like filament from which DNA binding sites protrude on the flexible linkers facilitating access. This filament-like nature of the intact H-NS has been observed in electron and scanning force microscopy-based studies reported elsewhere.<sup>19,20</sup> These studies showed H-NS being capable of bridging two adjacent strands of DNA. Our model can account for this occurrence, since two separate strands of DNA can be linked *via* the H-NS oligomer by running parallel with the line of the protein filament (see Figure 6).

## Materials and Methods

### Protein preparation

Expression vectors for the production of fragments of *Salmonella typhimurium* H-NS containing residues 1–57, 1–64, 12–89 were constructed as described.<sup>9</sup> The site-directed mutagenesis (Lys5Pro and Gln16Pro) on the 1–89 construct was performed using the QuikChange (Stratagene, CA, USA) method. All of these constructs as well as full length protein were expressed and purified as described elsewhere.<sup>9</sup> *E. coli* BL21 ( $\lambda$  DE3) pLys S cells were transformed with the plasmid encoding an N-terminal His<sub>6</sub>-tag polypeptide sequence as described.<sup>9</sup> As with previous experiments this construct had the wild-type residue Cys20, which is not highly conserved amongst the known sequences of bacterial H-NS homologues, replaced by a serine residue.<sup>7</sup> This substitution does not alter protein function but prevents disulphide formation under experimental conditions. Protein concentrations were determined using UV spectrometry employing extinction coefficients calculated from the number of tyrosine and tryptophan residues present.

For NMR spectroscopy samples <sup>15</sup>N and <sup>15</sup>N/<sup>13</sup>C isotope labelling was carried out by growing bacteria in M9 minimal medium using (<sup>15</sup>NH<sub>4</sub>)<sub>2</sub>SO<sub>4</sub>/<sup>12</sup>C<sub>6</sub>-glucose and (<sup>15</sup>NH<sub>4</sub>)<sub>2</sub>SO<sub>4</sub>/<sup>13</sup>C<sub>6</sub>-glucose as the sole nitrogen and carbon sources, respectively. The expression and purification of H-NS<sub>1–57</sub> was performed as reported for H-NS<sub>1–64</sub>.<sup>9,13</sup> All H-NS<sub>1–57</sub> samples were dissolved in 90% H<sub>2</sub>O/10% <sup>2</sup>H<sub>2</sub>O, containing 300 mM NaCl, 20 mM potassium phosphate, 1 mM EDTA, at pH 7.0. The monomer concentration of the protein ranged between 1 mM and 2 mM (estimated using a colorimetric assay). The NMR sample for the filtered/edited NOESY experiment was prepared by mixing equal concentrations of

unlabelled and <sup>15</sup>N/<sup>13</sup>C labelled polypeptides in 6 M urea, heated to the denaturation transition temperature of H-NS<sub>1–57</sub> (55 °C) for one hour and cooled slowly to room temperature. The mixture was exhaustively dialysed against the NMR buffer and spun to remove any precipitate before concentration for NMR analysis. The pattern of cross-peaks in the <sup>15</sup>N,<sup>1</sup>H-HSQC spectrum for the renatured sample was essentially identical with the fully labelled sample.

### Nuclear magnetic resonance (NMR) spectroscopy

NMR spectra were acquired on Varian UNITYplus 500 MHz, Varian UNITYplus 600 MHz and a Bruker AVANCE 800 MHz spectrometers at a temperature of 25 °C. The experiments recorded on <sup>15</sup>N labelled protein were 2D <sup>15</sup>N HSQC; 3D <sup>15</sup>N NOESY-HSQC,<sup>21</sup> 3D <sup>15</sup>N-separated TOCSY-HSQC.<sup>22</sup> The experiments recorded on <sup>15</sup>N/<sup>13</sup>C labelled samples were 3D <sup>13</sup>C-separated NOESY-HSQC,<sup>23</sup> <sup>13</sup>C HCCH-TOCSY,<sup>24</sup> HNCA, HNCOC, HN(CO)CA, HN(CA)CO; HNCACB; HN(CO)CACB.<sup>25</sup> A 100 ms 3D <sup>13</sup>C F<sub>1</sub>-filtered, F<sub>3</sub>-edited NOESY experiment<sup>15</sup> was recorded on a 2 mM sample of 1:1 unlabelled/<sup>13</sup>C,<sup>15</sup>N labelled HNS<sub>1–57</sub>. A mixing time of 80 ms was used in the NOESY experiments. The 3D <sup>15</sup>N-separated TOCSY-HSQC employed a mixing time of 60 ms, using the TOWNY sequence.<sup>26</sup>

Chemical shift calibrations for all nuclei were performed relative to the proton resonance of DSS as suggested.<sup>27</sup> Spectra were processed with NMRPipe<sup>28</sup> and analysed with AZARA 2.0<sup>29</sup> and ANSIG.<sup>30</sup>

### Structure calculation

Inter-proton distance restraints were derived from the ANSIG cross-peaks file of 3D <sup>15</sup>N-NOESY-HSQC, 3D <sup>13</sup>C-NOESY-HSQC and 3D <sup>13</sup>C F<sub>1</sub>-filtered, F<sub>3</sub>-edited NOESY-HSQC experiments. Some of the resonances were successfully assigned manually and the remaining peaks unassigned in one or more dimensions were given assignment possibilities on the basis of their chemical shifts using the “Connect” module from AZARA. The cross-peaks were grouped into four categories according to their relative peak intensities: strong, medium, weak and very weak and were designated with the corresponding distance restraint limit of 1.8–2.5 Å, 1.8–3.0 Å, 1.8–3.5 Å, 1.8–4.5 Å, respectively. 0.5 Å was added for distances that involved methyl groups.

The structure calculations were carried out using the PARALLHDGv5.1 parameter, with the non-bonded

energy function of PROLSQ<sup>31</sup> within the CNS program,<sup>16</sup> modified to allow floating stereochemistry of, and to include active swapping of, prochiral centers.<sup>32</sup> In order to lift the high ambiguity in the cross-peak assignment the initial calculations focused on the only coiled-coil region. The helical conformation was retained by using relatively high values for the dihedral force constant of 500 kcal mol<sup>-1</sup> rad<sup>-2</sup>. The ambiguous distance restraints were then filtered iteratively, based upon the coordinates of an ensemble of refined structures, and redundant restraints (duplicates) were discarded. Subsequently restraints relative to the remaining region of the protein were added and iteratively filtered. Due to the severe resonance overlap the final refined structure was calculated from a total of 1560 restraints of which 969 were unambiguous and 483 were ambiguous and 108 were from hydrogen bond (Table 1) with a dihedral force constant of 200 kcal mol<sup>-1</sup> rad<sup>-2</sup>. The unambiguous restraints were comprised of 868 intra-protomer and 101 inter-protomer restraints. The ambiguous restraints comprised 305 intra-protomer and 178 inter-protomer distances. Overall the unambiguous restraints comprised 466 intra-residue, 274 sequential, 126 medium-range and 103 long-range restraints and inter-chain entries. The elongated shape of the coiled-coil structure results in a lower number of long-range NOE contacts compared to globular proteins of the same molecular mass.

The programs TALOS<sup>33</sup> and CSI<sup>34</sup> were used to predict, from the backbone atom chemical shifts, upper and lower bounds for the  $\phi$  and  $\psi$  backbone torsion angles and the hydrogen bonding pattern for H-NS<sub>1-57</sub>. A total of 78 dihedral angle and 54 hydrogen bond inter-atomic distance (two per H-bond) restraints were used per protomer. The hydrogen bond and backbone torsion angle restraints restrict residues 2–5, 11–18 and 22–49 to  $\alpha$ -helical conformation.

#### Analytical size exclusion chromatography

Analytical SEC was performed on an ÄKTA FPLC using a Superose 12 HR10/30 (Pharmacia) operated at room temperature. All proteins were dialysed against 20 mM KPi buffer pH 7.0 containing 300 mM NaCl. 100  $\mu$ l of the sample were injected onto the column at a flow rate of 0.3 ml/min. Elution was monitored by UV absorption at 280 nm. A calibration of the expected flow rates was obtained using molecular mass standards (BioRad Gel Filtration Standard). Where appropriate polypeptide solutions were incubated at the required temperature in a thermostatted waterbath.

#### Analytical ultracentrifugation

Sedimentation equilibrium AUC measurements were performed in a Beckman XLA analytical ultracentrifuge using rotor number An 60 Ti. The pathlength of the cell was 1.2 cm. Typically, protein solutions at two to three different concentrations in 2 mM Tris-HCl (pH 8.0), 0.3 M NaCl and 0.68 M glycerol were allowed to reach equilibrium at three to four different speeds (including 20,000 rpm, 32,000 rpm, 36,000 rpm and 42,000 rpm). When equilibrium had been reached, radial measurements of the absorbance (at 280 nm or 240 nm) were made at 0.003 cm intervals based on averaging five readings. The data from different rotor speeds and concentrations were globally fitted to a single species model using the Beckman XLA/XLI software using the partial specific volume calculated from the amino acid content

and solvent density calculated from the solvent composition.

#### Protein Data Bank accession numbers

The coordinates have been deposited in PDB code 1LR1.

#### Acknowledgements

J.E.L. is a Wellcome Trust Senior Research Fellow. This work was funded by grants from the BBSRC (D.E., J.E.L., P.C.D., R.H.) and the Wellcome Trust (J.C.D.H., C.F.H.), the MRC (C.F.H.) and is a contribution from the BBSRC Bloomsbury Centre for Structural Biology. The authors thank Dr D. Nietlisplach, BBSRC National 800 MHz NMR Centre, University of Cambridge, UK and Dr B. Smith, Institute of Cell and Molecular Biology, University of Edinburgh, UK.

#### References

- Drlica, K. & Rouviere-Yaniv, J. (1987). Histone-like proteins of bacteria. *Microbiol. Rev.* **51**, 301–319.
- Higgins, C. F., Dorman, C. J., Stirling, D. A., Waddell, L., Booth, I. R., May, G. & Bremer, E. (1988). A physiological role for DNA supercoiling in the osmotic regulation of gene expression in *S. typhimurium* and *E. coli*. *Cell*, **52**, 569–584.
- Hulton, C. S. J., Seirafi, A., Hinton, J. C. D., Sidebotham, J. M., Waddell, L., Pavitt, G. D. *et al.* (1990). Histone-like protein H1 (H-NS), DNA supercoiling and gene expression in bacteria. *Cell*, **63**, 631–642.
- Hinton, J. C. D., Santos, D. S., Seirafi, A., Hulton, C. S. J., Pavitt, G. D. & Higgins, C. F. (1992). Expression and mutational analysis of the nucleoid-associated H-NS protein of *Salmonella typhimurium*. *Mol. Microbiol.* **6**, 2327–2337.
- Tupper, A. E., Owen-Hughes, T. A., Ussery, D. W., Santos, D. S., Ferguson, D. J. P., Sidebotham, J. M. *et al.* (1994). The chromatin-associated protein H-NS alters DNA topology *in vitro*. *EMBO J.* **13**, 258–268.
- Hommais, F., Krin, E., Laurent-Winter, C., Soutourina, O., Malpertuy, A., Le Caer, J.-P. *et al.* (2001). Large-scale monitoring of pleiotropic regulation of gene expression by the prokaryotic nucleoid-associated protein, H-NS. *Mol. Microbiol.* **40**, 20–36.
- Dorman, C. J., Hinton, J. C. D. & Free, A. (1999). Domain organization and oligomerization among H-NS-like nucleoid-associated proteins in bacteria. *Trends Microbiol.* **7**, 124–128.
- Ueguchi, C., Suzuki, T., Yoshida, T., Tanaka, K. & Mizuno, T. (1996). Systematic mutational analysis revealing the functional domain organization of *Escherichia coli* nucleoid protein H-NS. *J. Mol. Biol.* **263**, 149–162.
- Smyth, C. P., Lundbäck, T., Renzoni, D., Siligardi, G., Beavil, R., Layton, M. *et al.* (2000). Oligomerization of the chromatin-structuring protein H-NS. *Mol. Microbiol.* **36**, 962–972.
- Pon, C. L., Calogero, R. A. & Gualerzi, C. O. (1988). Identification, cloning, nucleotide-sequence and

- chromosomal map location of HNS, the structural gene for *Escherichia coli* DNA-binding protein H-NS. *Mol. Gen. Genet.* **212**, 199–202.
11. Ueguchi, C., Seto, C., Suzuki, T. & Mizuno, T. (1997). Clarification of the dimerization domain and its functional significance for the *Escherichia coli* nucleoid protein H-NS. *J. Mol. Biol.* **274**, 145–151.
  12. Williams, R. M., Rimsky, S. & Buc, H. (1996). Probing the structure, function, and interactions of the *Escherichia coli* H-NS and StpA proteins by using dominant negative derivatives. *J. Bacteriol.* **178**, 4335–4343.
  13. Renzoni, D., Esposito, D., Pfuhl, M., Hinton, J. C. D., Higgins, C. F., Driscoll, P. C. & Ladbury, J. E. (2001). Structural characterization of the N-terminal oligomerization domain of the bacterial chromatin-structuring protein, H-NS. *J. Mol. Biol.* **306**, 1127–1137.
  14. Lipari, G. & Szabo, A. (1982). Model-free approach to the interpretation of nuclear magnetic resonance relaxation in macromolecules: theory and range of validity. *J. Am. Chem. Soc.* **104**, 4546–4559.
  15. Zwahlen, C., Legault, P., Vincent, S. J. F., Greenblatt, J., Konrat, R. & Kay, L. E. (1997). Methods for measurement of intermolecular NOEs by multi-nuclear NMR spectroscopy: application to a bacteriophage lambda N-peptide/boxB RNA complex. *J. Am. Chem. Soc.* **119**, 6711–6721.
  16. Brünger, A. T., Adams, P. D., Clore, G. M., DeLano, W. L., Gro, P. & Grosse-Kunstleve, R. W. (1998). Crystallography and NMR system: a new software suite for macromolecular structure determination. *Acta Crystallog.* **54**, 905–921.
  17. Schröder, O., Tippner, D. & Wagner, R. (2001). Toward the three-dimensional structure of the *Escherichia coli* DNA-binding protein H-NS: a CD and fluorescence study. *Biochem. Biophys. Res. Commun.* **282**, 219–227.
  18. Dame, R. T., Wyman, C. & Goosen, N. (2000). H-NS mediated compaction of DNA visualized by atomic force microscopy. *Nucl. Acids Res.* **28**, 3504–3510.
  19. Schneider, R., Lurz, R., Lüder, G., Tolksdorf, C., Travers, A. & Muskhelishvili, G. (2001). An architectural role of the *Escherichia coli* chromatin protein FIS in organizing DNA. *Nucl. Acids Res.* **29**, 5107–5114.
  20. Dame, R. T., Wyman, C., Wurm, R., Wagner, R. & Goosen, N. (2002). Structural basis for H-NS-mediated trapping of RNA polymerase in the open initiation complex at the *rrnB* P1. *J. Biol. Chem.* **277**, 2146–2150.
  21. Ikura, M., Bax, A., Clore, M. & Gronenborn, A. M. (1990). Detection of nuclear Overhauser effects between degenerate amide proton resonances by heteronuclear three-dimensional nuclear magnetic resonance spectroscopy. *J. Am. Chem. Soc.* **112**, 9020–9021.
  22. Marion, D., Ikura, M., Tschudin, R. & Bax, A. (1989). Rapid recording of 2D NMR spectra without phase cycling. Application to the study of hydrogen exchange in proteins. *J. Magn. Reson.* **85**, 393–399.
  23. Zuiderweg, E. R. P., McIntosh, L. P., Dahlquist, F. & Fesik, S. W. (1990). Three-dimensional  $^{13}\text{C}$ -resolved proton NOE spectroscopy of uniformly  $^{13}\text{C}$  labeled proteins for the NMR assignment and structure determination of larger molecules. *J. Magn. Reson.* **86**, 210–215.
  24. Bax, A., Clore, M. & Gronenborn, A. M. (1990).  $^1\text{H}$ - $^1\text{H}$  correlation via isotropic mixing of  $^{13}\text{C}$  magnetization, a new three-dimensional approach for assigning  $^1\text{H}$  and  $^{13}\text{C}$  spectra of  $^{13}\text{C}$ -enriched proteins. *J. Magn. Reson.* **87**, 425–429.
  25. Yamazaki, T., Lee, W., Arrowsmith, C. H., Muhandiram, D. R. & Kay, L. A. (1994). Suite of triple resonance NMR experiments for the backbone assignment of  $^{15}\text{N}$ ,  $^{13}\text{C}$ ,  $^2\text{H}$  labelled proteins with high sensitivity. *J. Am. Chem. Soc.* **116**, 11655–11666.
  26. Kadkhodaei, M., Hwang, T. L., Tang, J. & Shaka, A. J. (1993). A simple windowless mixing sequence to suppress cross relaxation in TOCSY experiments. *J. Magn. Reson. ser. A*, **104**, 105–107.
  27. Wishart, D. S., Bigam, C. G., Yao, J., Abildgaard, F., Dyson, H. J., Oldfield, E. *et al.* (1995).  $^1\text{H}$ ,  $^{13}\text{C}$  and  $^{15}\text{N}$  chemical shift referencing in biomolecular NMR. *J. Biomol. NMR*, **6**, 135–140.
  28. Delaglio, F., Grzesisek, S., Vuister, G. W., Zhu, G., Pfeifer, J. & Bax, A. (1995). NMR-Pipe—a multi-dimensional spectral processing system based on UNIX pipes. *J. Biomol. NMR*, **6**, 277–293.
  29. Boucher, W. (1996). AZARA v2.0, Department of Biochemistry, University of Cambridge, UK.
  30. Kraulis, P. (1989). ANSIG: a program for the assignment of protein  $^1\text{H}$  2D NMR spectra by interactive graphics. *J. Magn. Reson.* **24**, 627–633.
  31. Linge, J. P. & Nilges, M. (1999). Influence of non-bonded parameters on the quality of NMR structures: a new force field for NMR structure calculation. *J. Biomol. NMR*, **13**, 51–54.
  32. Wakefield, R. I. D., Smith, B. O., Nan, X., Free, A., Soteriou, A. & Uhrin, D. (1999). The solution structure of the domain from MeCP2 that binds to methylated DNA. *J. Mol. Biol.* **291**, 1055–1065.
  33. Cornilescu, G., Delaglio, F. & Bax, A. (1999). Protein backbone angle restraints from searching a database for chemical shift and sequence homology. *J. Biomol. NMR*, **13**, 289–302.
  34. Wishart, D. S. & Sykes, B. D. (1994). The  $^{13}\text{C}$  chemical-shift index: a simple method for the identification of protein secondary structure using  $^{13}\text{C}$  chemical-shift data. *J. Biomol. NMR*, **4**, 171–180.
  35. Shindo, H., Iwaki, T., Ieda, R., Kurumizaka, H., Ueguchi, C. & Mizuno, T. (1995). Solution structure of the DNA-binding domain of a nucleoid-associated protein, H-NS, from *Escherichia coli*. *FEBS Letters*, **360**, 125–131.
  36. Laskowski, R. A., MacArthur, M. W. & Moss, D. S. (1993). Procheck—a program to check the stereochemical quality of protein structures. *J. Appl. Crystallog.* **26**, 283–291.

Edited by P. Wright

(Received 5 August 2002; received in revised form 7 October 2002; accepted 8 October 2002)